NISTIR 6872

Evaluation of Fire Models for Nuclear Power Plant Applications: Cable Tray Fires

International Panel Report

Compiled by Monideep K. Dey, Guest Researcher

National Institute of Standards and Technology
Technology Administration, U.S. Department of Commerce

NISTIR 6872

Evaluation of Fire Models for Nuclear Power Plant Applications: Cable Tray Fires

International Panel Report

Compiled by Monideep K. Dey, Guest Researcher
Fire Research Division
Building and Fire Research Laboratory

June 2002

U.S. DEPARTMENT OF COMMERCE
Donald L. Evans, Secretary
TECHNOLOGY ADMINISTRATION
Phillip J. Bond, Under Secretary of Commerce for Technology
NATIONAL INSTITUTE OF STANDARDS AND TECHNOLOGY
Arden L. Bement, Jr., Director

Appendix B: Benchmark Analysis with CFAST and FDS, Monideep DEY, NRC/NIST, USA

SUMMARY

This Appendix presents analyses conducted with the CFAST and FDS fire models for an international benchmark exercise aimed at evaluating the capability of current fire models to simulate cable tray fires of redundant safety systems in nuclear power plants. The exercise involved simulating fire scenarios in a large nuclear power plant compartment with cable trays as targets in varying ventilation conditions. The analyses demonstrate that both the CFAST and FDS codes provide a treatment of most physical phenomena in the scenarios analyzed. The predicted time scale and magnitude of the main parameters of interest in these scenarios by both codes are similar. The sub-model for the target, and issues regarding the thermal environment of the target, are the largest source of uncertainty for these types of scenarios. It will be useful to conduct validation exercises for CFAST and FDS in which the predictive capability of target damage is the main focus of the validation. These exercises will provide information to allow the development of quantitative estimates of the uncertainties for the major parameters of interest.

INTRODUCTION

The analysis presented in this Appendix was conducted as part of a benchmark exercise in the International Collaborative Project to Evaluate Fire Models for Nuclear Power Plant Applications (Dey, 2000). The objective of the collaborative project is to share the knowledge and resources of various organizations to evaluate and improve the state of the art of fire models for use in nuclear power plant fire safety and fire hazard analysis. The project is divided into two phases. The objective of the first phase is to evaluate the capabilities of current fire models for fire safety analysis in nuclear power plants. The second phase will implement beneficial improvements to current fire models that are identified in the first phase, and extend the validation database of those models. Currently, twenty-two organizations from six countries are represented in the collaborative project.

The first task of the international collaborative project is to evaluate the capability of fire models to analyze cable tray fires of redundant safety systems in nuclear power plants. The safety systems are required to safely shutdown the reactor during abnormal and emergency events in the plant. A specified distance separates cable trays of redundant safety systems if they are located in the same compartment in which a single fire could potentially damage both systems. Therefore, the analysis of fires that could damage redundant safety trains is an important part of nuclear power plant fire hazard analysis. The evaluation of the capability of fire models to analyze these scenarios is being conducted through an international benchmark exercise.

The benchmark exercise (Bertrand and Dey, 2001) is intended to simulate a basic scenario defined in sufficient detail to allow evaluation of the physics modeled in the fire computer codes. An assessment of appropriate input parameters and assumptions, interpretation of results, and determining the adequacy of the physical sub-models in the codes for specific scenarios will establish useful technical information regarding the capabilities and limitations of the fire computer codes. This valuable information will be documented in a technical reference manual for fire model users. Generic insights regarding the capabilities of the models will also be developed in this process and documented. The comparisons between codes can be used to understand the modeling of the physics in them, i.e. if all the codes

produce similar results over a range of scenarios then the physics modeled in the codes is probably adequate for this scenario. However, the compounding effects of different phenomena will also need to be examined as part of this evaluation. Some variations in the results may be acceptable depending on how the results will be used. Uncertainties in the predictions based on validations of each code will provide a basis for the confidence on the set of results developed in the exercise.

This Appendix presents the analyses for the benchmark exercise conducted using the Consolidated Fire And Smoke Transport [CFAST] (Jones, 2000), and Fire Dynamic Simulator [FDS] (McGrattan, 2000) computer codes developed by the National Institute of Standards and Technology, U.S. Department of Commerce. The paper provides the results of an assessment and verification of the capability of these computer codes to analyze the fire scenario specified for the benchmark exercise.

DEFINITION OF SCENARIO

A representative emergency switchgear room for a Pressurized Water Reactor (PWR) has been selected for this benchmark exercise. The room is 15.2 m (50 ft) deep x 9.1 m (30 ft) wide and 4.6 m (15 ft) high. The room contains the power and instrumentation cables for the pumps and valves associated with redundant safety systems. The power and instrument cable trays run the entire depth of the room, and are separated horizontally by a distance, d. The cable trays are 0.6 m (≈24 in) wide and 0.08 m (≈3 in) deep. A simplified schematic of the room, illustrating critical cable tray locations, is shown in Figure 1. The room has a door, 2.4 m x 2.4 m (8 ft x 8 ft), and a mechanical ventilation system with a flow rate of 5 volume changes per hour in and out of the room.

There are two parts to the exercise. The objective of Part I is to determine the maximum horizontal distance between a specified transient (trash bag) fire and tray A that results in the ignition of tray A. Part II examines whether the target cable tray B will be damaged for several heat release rates of the cable tray stack (A, C2, and C1), and horizontal distance, d. The effects of the fire door being open or closed, and the mechanical ventilation on or off, are examined in both parts of the benchmark exercise.

VALIDATION OF THE CFAST AND FDS FIRE CODES

The CFAST and FDS fire codes have been compared to several data sets from experiments, including those with configurations and fire intensities similar to that specified for the benchmark exercise. However, none of the tests included cable trays as target material to measure the response of the target to the physical environment in the compartment.

Results from the CFAST code have been compared to several tests of fires in spaces ranging from small compartments to large aircraft hangers. Peacock (1993) compared predictions of CFAST to four fire tests in a single compartment, multi-compartment on a single floor, and a seven-story building. The magnitude and trends (time to critical conditions and general curve shape) are reported. The comparisons ranged from a few percent to a factor of 2 to 3 of the measured values.

Results from the FDS code, Version 1, has been compared with experimental data for open plumes, back draft, flashover, a warehouse fire, pool fires in a Navy Hangar, and fires in a decommissioned nuclear reactor containment. These comparisons demonstrated the enhanced predictive capability of this code for a wide range of fire scenarios, and also identified areas for improvement. Specifically, the modeling of radiation from the hot gases and walls is an important effect in nuclear power plant compartment fires. The modeling of this effect has been included in Version 2, which was released in December 2001. Significant improvements in the predictions of the tests in the decommissioned containment building have been achieved with FDS, Version 2.

Although several comparisons of these codes to experimental data are available, it is not possible at this stage to translate this research to quantitative estimates of uncertainties of the predicted results from the codes for the benchmark exercise. A complete analysis of past validation research, including an examination of the effect of the specifics (compartment configuration, fire source intensity, ventilation, etc.) of a fire scenario on the predictive capability of the codes is planned.

RESULTS OF THE ANALYSES

Part I

CFAST Analyses

The major sub-models used in CFAST for the scenarios specified in the benchmark exercise are (1) combustion chemistry (tracking O_2, and species); (2) plumes and layers; (3) vent flow, including forced ventilation; and (4) heat transfer, especially radiation and convection to the target.

The following presents the major highlights of the results obtained for the analysis of the benchmark exercise. The trends of various parameters are examined to verify the adequacy of the basic sub-models for the specific scenarios. The general conclusions from the exercise are also presented, although as indicated above, quantitative estimates of the uncertainties associated with the predictive capability of the codes for the specific parameters examined are not available at this time.

The measured heat release rate (Lee, 1985) of a large trash bag was used as input for the simulation as shown in Figure 2. In order to conduct a simplified and conservative analysis, the target is assumed to be a single power cable with a diameter of 50 mm at the bottom left corner of the cable tray A. Consistent with the target models in CFAST and FDS, the target cable is represented as a rectangular slab oriented horizontally with a thickness of 50 mm. The cable is assumed to ignite when the centerline of the cable reaches 643 K. Table 1 summarizes the cases for Part I of the benchmark exercise. The peak heat release for the trash bag fire (Figure 2) for Part I is $\approx$ 350 kW, and peaks at $\approx$ 150 s.

Table 1. Summary of Cases for Part I

	Distance between Trash Bag & Cable	Door	Ventilation System
Base Case	2.2 m	Closed*	Off
Case 1	0.3+		
Case 2	0.9		
Case 3	1.5		
Case 4		Open	
Case 5			On

* For simulations with the door closed, a crack (2.4 m x 0.005 m) at the bottom of the doorway was assumed.

+A value in a cell indicates the parameter was varied from the base case.

Base Case

Figure 3 shows the predicted oxygen depletion for the Base Case. The oxygen concentration in the lower layer stays approximately constant, as would be expected. The oxygen concentration in the upper layer decreases by ≈ 1 % to 19.2 %. Therefore, the fire will not be limited by oxygen in this fire scenario.

Figure 2 also shows the plume flow development during this scenario. The main plume flow increases rapidly at the initiation of the fire, and does not follow the fire heat release rate, as expected. CFAST over predicts mass entrainment at the initial stages of the fire because of the plume height used in the calculation of the entrained air. Initially, the plume height is assumed to be from the fire to the ceiling. This leads to an over prediction of the initial mass flow to the upper layer, and the rate of descent of the gas layer interface.

Figure 4 shows the hot gas layer (HGL) temperature and the interface height development. The upper layer temperature peaks at ≈ 230 s, about 80 s after the fire peaks, due to the lag time for the heating of the gas by the fire. In this scenario, the upper layer temperature increases only about 50 K. After peaking, the upper layer temperature decreases with time due to the heat loss to the boundaries. The interface height decreases rapidly initially due to high plume flow (see Figure 2). The rate of descent of the interface height decreases after ≈ 230 s when the HGL temperature has peaked. The hot gas layer is prevented from reaching the floor due to air inflow at the crack below the door caused by a negative pressure in the compartment (see Figure 5).

Figure 5 shows the pressure development, and the resulting flows in and out of the compartment. The pressure peaks at ≈ 150 s when the fire heat release rate peaks, as would be expected. The pressure decreases after the fire peaks due to outflow from the compartment at the crack under the door, and swings to a negative value. The small oscillations in the pressure after ≈ 250 s is due to the small fluctuations in the heat release rate. The peak in the outflow is consistent with the pressure profile, and the outflow goes to zero when the pressure in the compartment is less than the outside. The initiation of inflow is consistent with the pressure profile, and is much less than the outflow. The small oscillation of the inflow is caused by the fluctuations in the pressure.

Figure 6 shows the components of the heat flux to the target. The radiative flux on the target from the fire follows the fire heat release rate curve, as expected. The radiative flux on the target (lower side) from the hot gas increases at the point (≈ 100 s) when the interface height reaches the target. The radiative flux from the hot gas on the target peaks at ≈ 280 s, 50 s after the upper layer temperature peaks, and decreases in a similar manner to the upper layer temperature. The lag between the peak in the radiative flux from the hot gas and the upper layer temperature is because of the time needed for hot gas layer growth under the target. The convective flux is negative initially because the target temperature is greater than the lower layer temperature. The convective flux becomes positive and starts to increase at ≈ 100 s when the hot gas layer interface reaches the target, as expected. The convective flux peaks at ≈ 230 s when the upper layer temperature peaks, as expected.

Cases 1 to 3

Figure 7 shows the target surface temperatures versus time for the Base Case and Cases 1 -3. For the Base Case, the target temperature peaks at ≈ 290 s, ≈ 140 s after the fire and target flux reaches its peak due to the thermal inertia of the target. The target surface temperature only increases ≈ 20 K for this case. Figure 8 is a plot of the maximum surface temperatures of the target versus the distance between the fire and target. The plot could be approximated by a straight line and does not show a rapid increase in temperature with decreasing distance between the fire and the target. This can be explained by examining Case 1. The radiative flux from the hot gas layer is the same as the Base Case since the only difference between the cases is the fire location. The radiation from the fire is the largest in Case 1 because the fire is closest to the target; however, the peak convective flux is half of that in the Base Case (100 vs. 200 W/m^2). The decreased peak convective flux is caused by a smaller difference in temperature between the hot gas layer and the target surface (the target surface temperature is higher due to higher radiative flux).

Cases 4 and 5

The following presents some key features of the results of Case 4 and 5. Figure 9 shows the development of the interface height for Case 4 versus the Base Case. The interface height approaches a constant value at ≈ 140 s, after the HGL reaches the top of the door at ≈ 100 s. Figure 10 shows the development of the upper layer outflow and lower layer inflow after the HGL interface reaches the door at ≈ 100 s, indicating the establishment of a neutral plane below the top of the door (at ≈ 2.2 m). Figure 11 shows the HGL temperature development for Case 4 and 5. The HGL temperature for Case 4 is less than the Base Case after ≈ 270 s because of the outflow of hot gas from the upper layer (which reaches its peak value at ≈ 200 s) through the door, and higher plume flow. The HGL temperature for Case 5 is less than that in the Base Case after ≈ 100 s when the HGL reaches the mechanical vents, and ambient air is injected into and hot gas ejected from the hot gas layer.

Figure 12 shows the development of flows in the mechanical ventilation system for Case 5. The transitions in flows from the mechanical vents in and out of the gas layers occurs at about ≈ 100 s when the HGL reaches the mechanical vents. The mass flow rate into the upper layer is larger than the mass flow rate out of the upper layer because mechanical

ventilation flows in CFAST are specified as volumetric flow rates. The temperature of the flow out of the compartment is higher than the ambient conditions of the flow into the compartment. Figure 3 shows that the oxygen concentration in the HGL layer is greater in Case 5 than the Base Case after ≈ 160 s when the HGL reaches the mechanical vents, and air at ambient conditions is injected in to the upper layer. Figure 7 shows the target surface temperature for Case 4 and 5 along with the other cases. The target surface temperature for Case 4 and 5 is less than in the Base Case because of cooler hot gas layer temperatures. The cable temperature does not approach the point of ignition (643 K) in any of the cases analyzed.

The above analyses of the results for Part 1 demonstrates that CFAST provides a treatment of most physical phenomena of interest in the scenarios analyzed. The results indicate that the trends predicted by the sub-models in CFAST are reasonable and provide insights beneficial for nuclear power plant fire safety engineering.

FDS Analyses

The following presents a summary of the analyses that was conducted with the FDS code in order to allow a comparison with the results from CFAST. Direct comparison between CFAST and FDS for several parameters discussed above is difficult. The total flow through vents is not a direct output from the FDS code. Plume flow and the hot gas layer interface height are computed directly in a zone model, but not in CFD models.

Figure 13 is an output image from the Smokeview (Forney, 2000) graphical interface to the FDS code, which allows a comprehensive visual analysis of the code output. The specific image in Figure 13 is a slice file, which shows the development of system parameters versus time for a particular plane in the 3-D geometry simulated. This specific figure shows a snapshot of the temperature profile at the midpoint of the room (where the trash bag is located) for the Base Case at 230 s. Although it is not possible to obtain an accurate determination of the interface height from images such as shown in Figure 13, a visual examination of the slice file versus time showed that the time scales for hot gas layer development and peak temperatures (at ≈ 230 s for the Base Case, Case 4, and Case 5) predicted by CFAST and FDS are similar. Similar observations of the pressure slice file simulations indicated that the magnitude and timing of the pressure peak (at ≈ 150 s for the Base Case) were also similar.

Figure 14 is a vector plot of temperature in a plane parallel to the cable trays at the midpoint of the room (and door) and illustrates the flow patterns for Case 4 in which the door is open. Outflow and inflow at the door around the neutral plane is illustrated, as also predicted by the CFAST code. Figure 15 is a similar plot in a plane perpendicular to the cable trays at the midpoint of the room (and fire) and illustrates the flow patterns caused by the mechanical ventilation system in Case 5. This information will be necessary to examine the local effects of target heating.

One important difference in the results from the CFAST and FDS codes for the type of scenarios examined for the Benchmark Exercise is the hot gas temperature. CFAST, a two-zone code, calculates the *average* temperature of the hot gas layer, whereas FDS computes the entire temperature profile in the compartment. The peak average HGL temperature (at ≈

275 s) predicted by CFAST for the Base Case is 77 C. The temperature profile predicted by FDS for this case (at ≈ 275 s) ranged from 75 C in the lower region to 130 C in the upper region of the hot gas. This temperature gradient in the hot gas will determine the convective heat flux to the cable tray depending on its vertical position. Table 2 compares the results obtained from the CFAST and FDS codes. Most of the results are similar. The largest difference is noted for the convective heat flux to the target in the Base Case. This is expected because the vertical temperature gradient would be the largest for this case with no ventilation. The differences in the target surface temperatures calculated for all the cases analyzed are within 20 %.

Table 2. Comparison of CFAST and FDS Results

	Max. Rad. Flux (w/m^2) At Target		Max. Conv. Flux (w/m^2) At Target		Max. Target Surface Temp. (K)	
	CFAST	FDS	CFAST	FDS	CFAST	FDS
Base Case	587	712	188	485	322	333
Case 4	582	704	186	277	321	325
Case 5	588	710	148	180	318	319

Part II

The following presents the results of analyses with the CFAST code. Due to time constraints, FDS was not exercised for Part II of the benchmark Exercise.

Predicting the heat release rate of a burning cable tray stack is extremely complex, therefore, the mass loss rate of the burning cable tray stack was defined as input in the exercise. The consecutive ignition and burning of all 3 cable trays (trays A, C2, and C1) were modeled as one fire. The analyses were conducted assuming a peak heat release rate for the whole cable tray stack between 1 – 3 MW. A t-squared fire growth with t_0 = 10 min., and Q_0 = 1 MW was assumed, where:

$$Q=Q_0 (t/t_0)^2$$

The cable fire was assumed to last for 60 minutes at the peak heat release rate, and decay in a t-squared manner with similar constants as for growth.

The heat source (trays A, C2, and C1) was assumed to be at the center of the cable tray length and width and at the same elevation as the bottom of tray C2. The target (representing tray B) was assumed to be at the center of the cable tray length. In order to conduct a simplified and conservative analysis, the target was assumed to be a single power or instrumentation cable, without an electrical conductor inside the cable, and with a diameter of 50 mm or 15 mm respectively at the bottom right corner of cable tray B. The target in CFAST is modeled as a rectangular slab, and was assumed to be horizontally oriented with a thickness of 50 mm or 15 mm. The cable was assumed to be damaged when the centerline of the cable reached 473 K.

Table 3 summarizes the cases for Part II of the benchmark exercise.

Table 3 Summary of Cases for Part II

Fire Scenario	HRR (MW)	D (m)	Door Position	Mech. Vent. Sys.	Target	Target Elev. (m)
Base Case	1	6.1	Closed*	Off	Power Cable	1.1
Case 1		3.1+				
Case 2		4.6				
Case 3	2	3.1				
Case 4	2	4.6				
Case 5	2	6.1				
Case 6	3	3.1				
Case 7	3	4.6				
Case 8	3	6.1				
Case 9			Open>15 min	Off>15 min		
Case 10			Open	On		
Case 11						2.0
Case 12						Same
Case 13					Instrument Cable	

* For simulations with the door closed, a crack (2.4 m x 0.005 m) at the bottom of the doorway was assumed.

+A value in a cell indicates the parameter is varied from the base case.

Base Case

Figures 16 to 20 show the predicted results of the main parameters of interest. Figure 21 shows the pyrolysis rate specified for the case. The predicted trend for the heat release rate, interface height, and oxygen concentration in Figures 16, 17, and 18 is collectively examined. CFAST predicts that the HGL interface lowers to the fire source (at an elevation of 3.4 m) at ≈ 580 s. The heat release rate decreases rapidly at this time since the oxygen concentration in the HGL is lower than the specified lower oxygen limit of 12 %. The interface height increases at this point due to inflow into the lower layer from the outside caused by a rapid reduction in the heat release rate and pressure. The heat release rate increases after this point due to the fluctuations in the interface height that temporarily expose the fire source to sufficient oxygen in the lower layer. After ≈ 600 s, the interface height starts to decrease slowly as a result of continued pyrolysis and the production of hydrocarbons.

The HGL profile shown in Figure 19 is consistent with the HRR profile shown in Figure 16. The HGL temperature reaches its peak of ≈ 440 K at ≈ 600 s when the HRR peaks, and decreases rapidly with the heat release rate. The HGL approaches ambient conditions at ≈ 1200 s shortly after the HRR goes to zero. The target surface temperature is shown in Figure 20 and peaks at ≈ 600 s at a value 323 K, only 23 K above ambient conditions. The target temperature then decreases at a less rapid rate than the HGL temperature due to the thermal inertia of the PVC cable.

The above analysis demonstrates the complexity in modeling an elevated fire source which can be affected by a limited oxygen environment. The assumption for the LOL will have a significant effect on the predicted peak target temperature. Conservative assumptions are warranted due to the uncertainty in the extinction model used in CFAST.

Cases 1 and 2

Analysis of the results for Cases 1 and 2 showed that the distance between the fire and target did not have a strong effect on the target temperature. The absence of the typical strong effect of the distance between the fire and target due to the radiative flux incident on the target was discussed earlier.

Cases 3 to 8

As discussed above, the cable tray fire in the Base Case is limited by the oxygen depletion in the environment. Cable tray fires that could be potentially more intense (as specified by the pyrolysis rate for these cases) are also limited, i.e., the HRRs are similar to that specified for the Base Case. Therefore, these cases are not discussed further here.

Special Case

Since the fire was extinguished after ≈ 720 s and well before 4800 s, the expected duration of the fire, a special case was analyzed. The special case was the same as the Base Case, except the fire was located at an elevation below the top of the door at 1.8 m, and the door was open. Natural ventilation of the hot gases through the door prevented the HGL from reaching and extinguishing the cable tray fire. Therefore, a fire that was sustained at the specified intensity for 3600 s was achieved. Figure 22 shows the HGL and target surface temperature development. The HGL and target surface temperatures peaked at 457 K and 435 K.

CONCLUSIONS

The above analyses of the benchmark exercise for cable tray fires of redundant safety systems demonstrate that both the CFAST and FDS codes provide a treatment of most physical phenomena in the scenarios analyzed. For Part I, the time scale and magnitude of the development of the main parameters of interest in these scenarios are similar. The difference in the predicted target surface temperature between the codes is less than 20 % for the scenarios analyzed. Comparisons of these results with those obtained by others using different fire codes in the benchmark exercise will further verify the physical sub-models in these codes. Comparison of code results with data from a test series specifically focused on target damage would broaden the validation database of these codes.

The analysis of the scenarios in Part II demonstrate the complexity in modeling an elevated fire source that can be affected by a limited oxygen environment. The extinction sub-models utilized in CFAST is an approximation of the interaction of the complex combustion process with a limited oxygen environment. Therefore, the result from the extinction sub-model represents an approximation of the conditions expected for the fire scenarios. The assumption for the LOL will affect the predicted peak target temperature. Therefore, conservative assumptions are warranted due to the uncertainty in the extinction model.

It is concluded that the results obtained from these codes can provide insights beneficial for nuclear power plant fire safety analysis for the type of scenarios analyzed, if the limitations of the code is understood. Further analyses of different fire scenarios are planned. The sub-model for the target, and issues regarding the thermal environment of the target, are the largest source of uncertainty for the types of scenarios in Part I. It will be useful to conduct validation exercises for CFAST and FDS in which the predictive capability of target damage is the main focus of the validation. Also, more refined measurements and data analyses are needed to estimate the quantitative uncertainties of the parameters predicted in the analyses of these fire scenarios. The code results, with quantitative estimates of the uncertainties in the predicted parameters, should provide a sound basis for engineering judgments in nuclear power plant fire safety analysis.

REFERENCES

Dey, M.K., "International Collaborative Project to Evaluate Fire Models for Nuclear Power Plant Applications: Summary of Planning Meeting," NUREG/CP-0170, U.S. Nuclear Regulatory Commission, Washington, DC, April 2000.

Bertrand, R, and Dey, M.K., "International Collaborative Project to Evaluate Fire Models for Nuclear Power Plant Applications: Summary of 2nd Meeting," NUREG/CP-0173, U.S. Nuclear Regulatory Commission, Washington, DC, July 2001.

Floyd, J., "Comparison of CFAST and FDS for Fire Simulation with the HDR T51 and T52 Tests," NISTIR 6866, National Institute of Standards and Technology, Gaithersburg, Maryland, April 2002.

Forney, G.P., and McGrattan, K.B., "User's Guide for Smokeview Version 1.0 – A Tool for Visualizing Fire Dynamics Simulation Data," NISTIR 6513, National Institute of Standards and Technology, Gaithersburg, Maryland, May 2000.

Jones, W.W., Forney, G.P., Peacock, R.D., and Reneke, P.A., "A Technical Reference for CFAST: An Engineering Tool for Estimating Fire and Smoke Transport," NIST TN 1431, National Institute of Standards and Technology, Gaithersburg, Maryland, January 2000.

Lee, B. T., "Heat Release Rate Characteristics of Some Combustible Fuel Sources in Nuclear Power Plants," NBSIR 85-3195, National Bureau of Standards, 1985.

McGrattan, K.B., Baum, H.R., Rehm, R.G., Hamins, A., & Forney, G.P., "Fire Dynamics Simulator - Technical Reference Guide," NISTIR 6467, National Institute of Standards and Technology, Gaithersburg, Maryland, January 2000.

Peacock, R.D., W.W. Jones, and R.W. Bukowski, "Verification of a Model of Fire and Smoke Transport," *Fire Safety Journal*, Vol. 21, pp. 89–129, 1993.

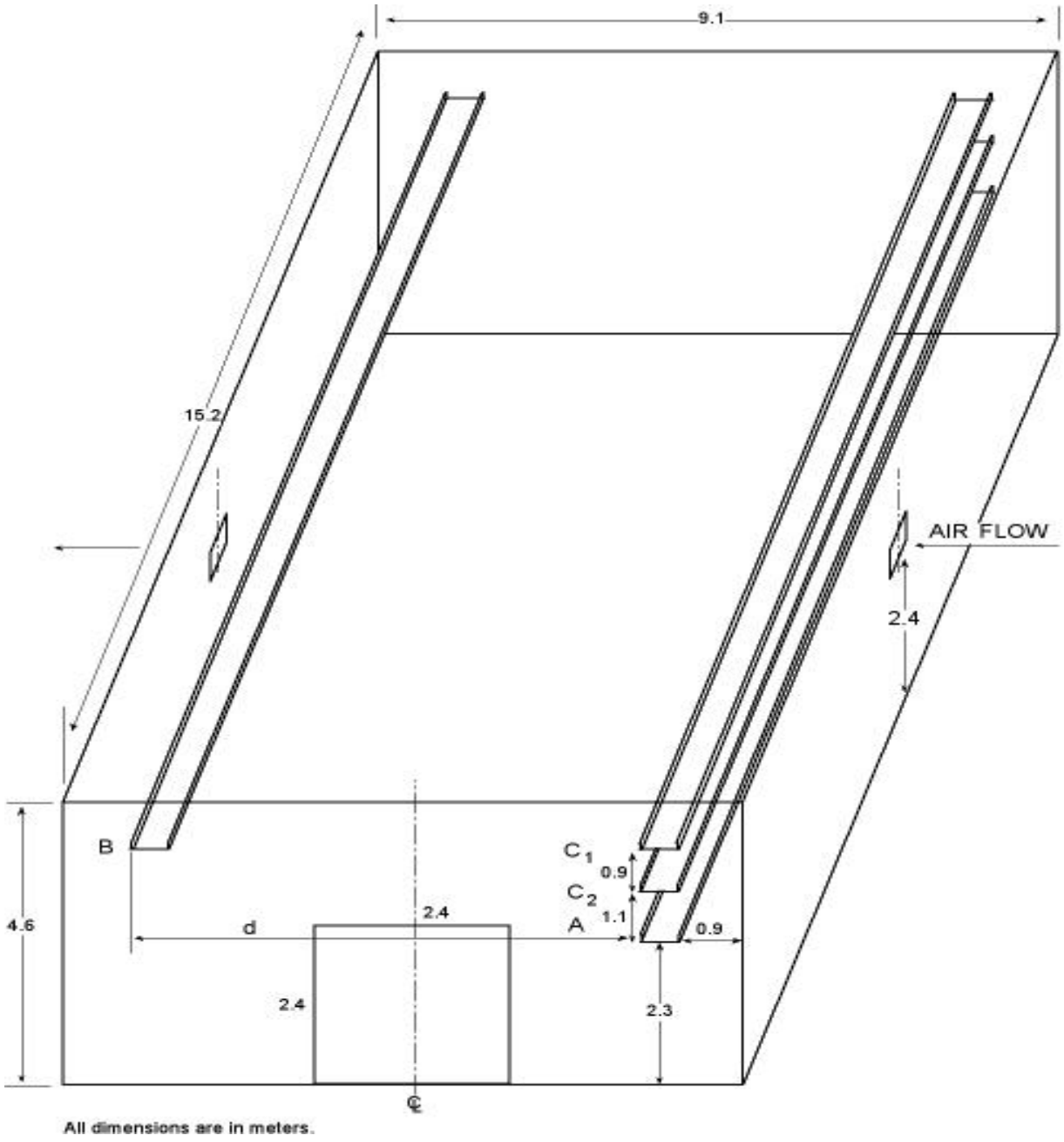

Figure 1 Schematic of PWR Room

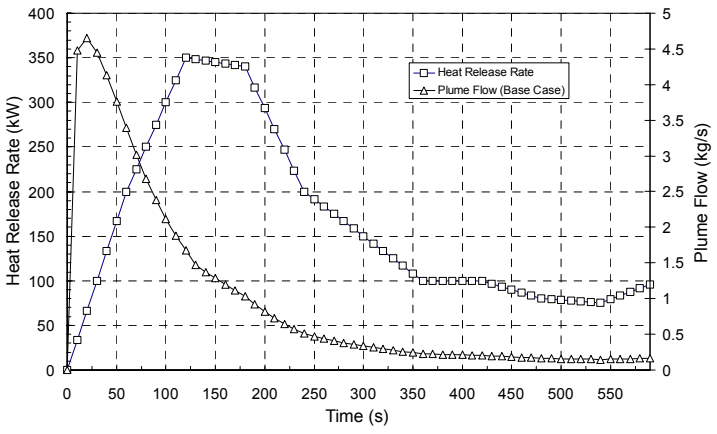

Figure 2 Heat Release Rate and Plume Flow

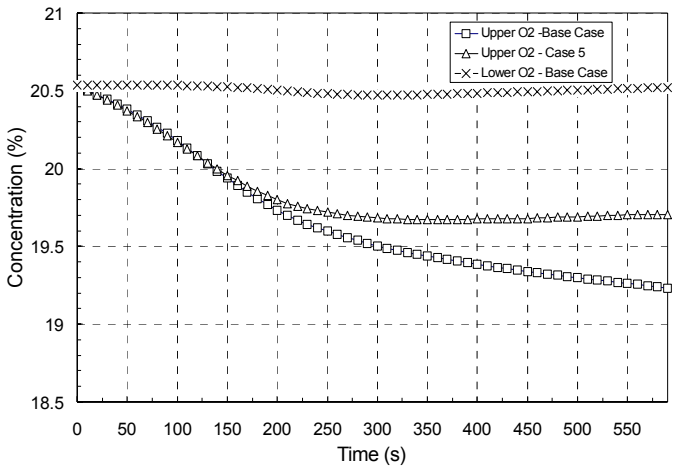

Figure 3 Oxygen Concentrations – Part I

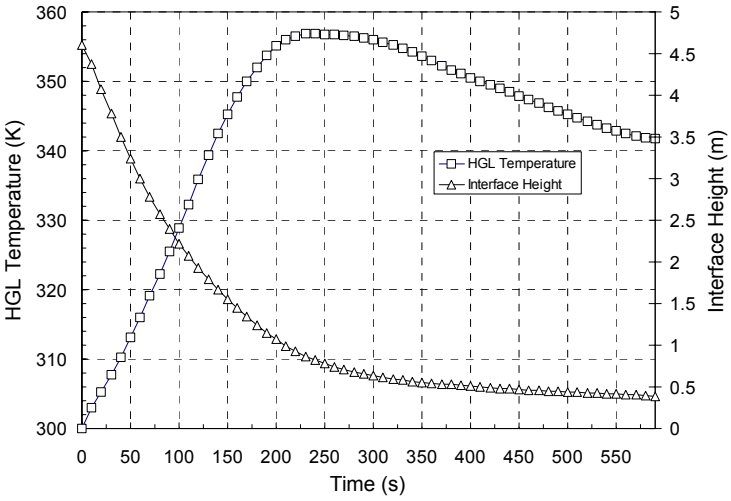

Figure 4 HGL Development – Base Case, Part I

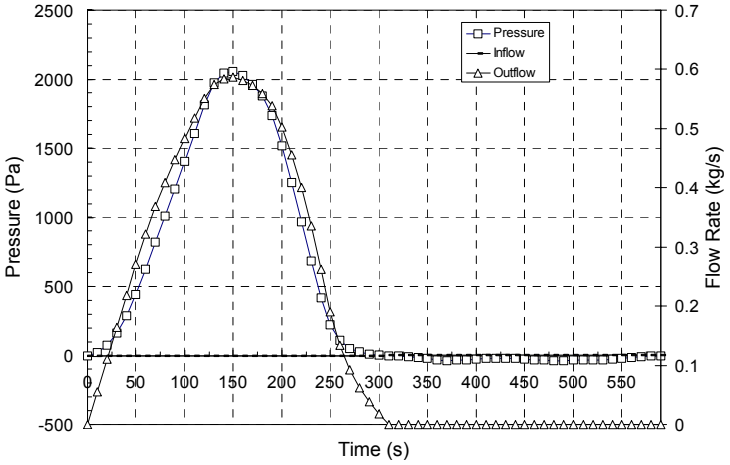

Figure 5 Pressure and Vent Flow Development – Base Case, Part I

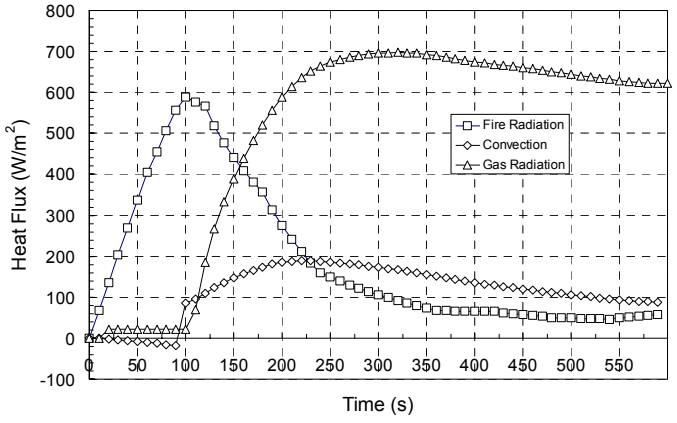

Figure 6 Heat Fluxes – Base Case, Part I

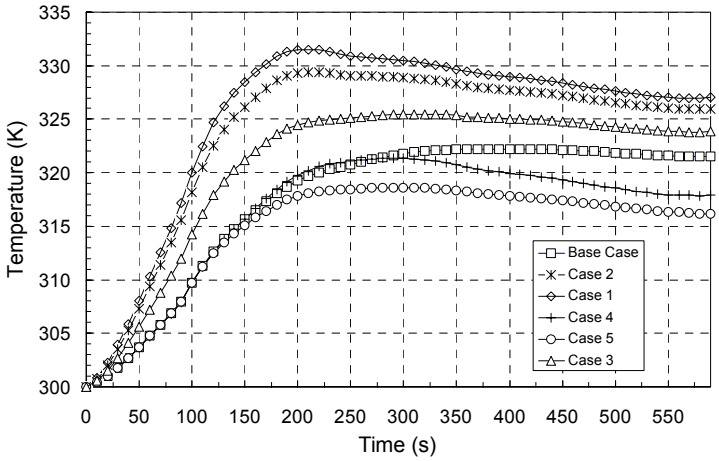

Figure 7 Target Surface Temperatures, Part I

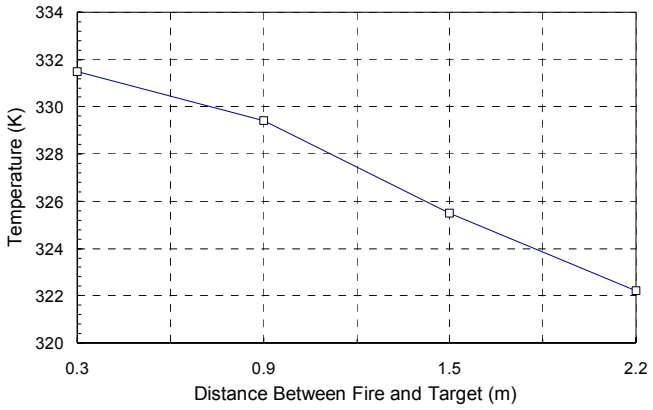

Figure 8 Target Surface Temperatures, Part I

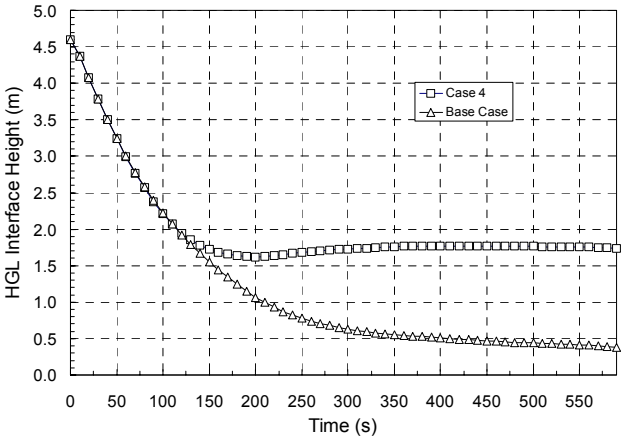

Figure 9 HGL Development – Case 4, Part I

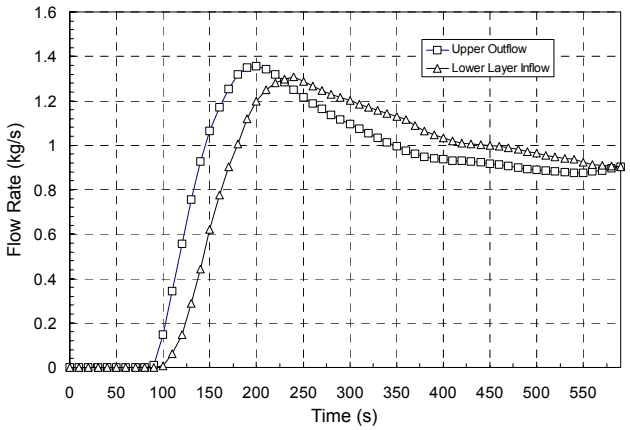

Figure 10 Door Flows – Case 4, Part I

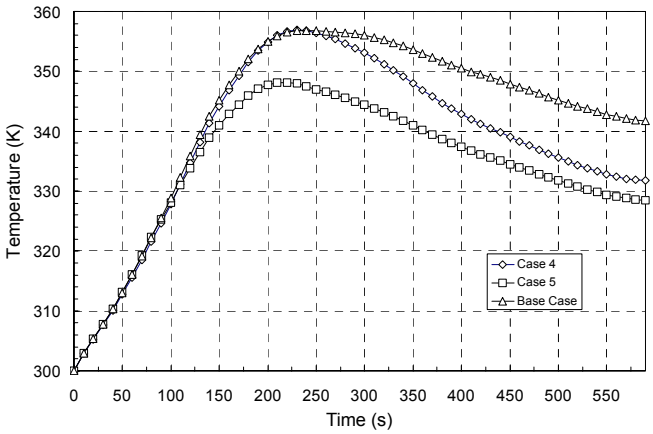

Figure 11 HGL Temperature, Part I

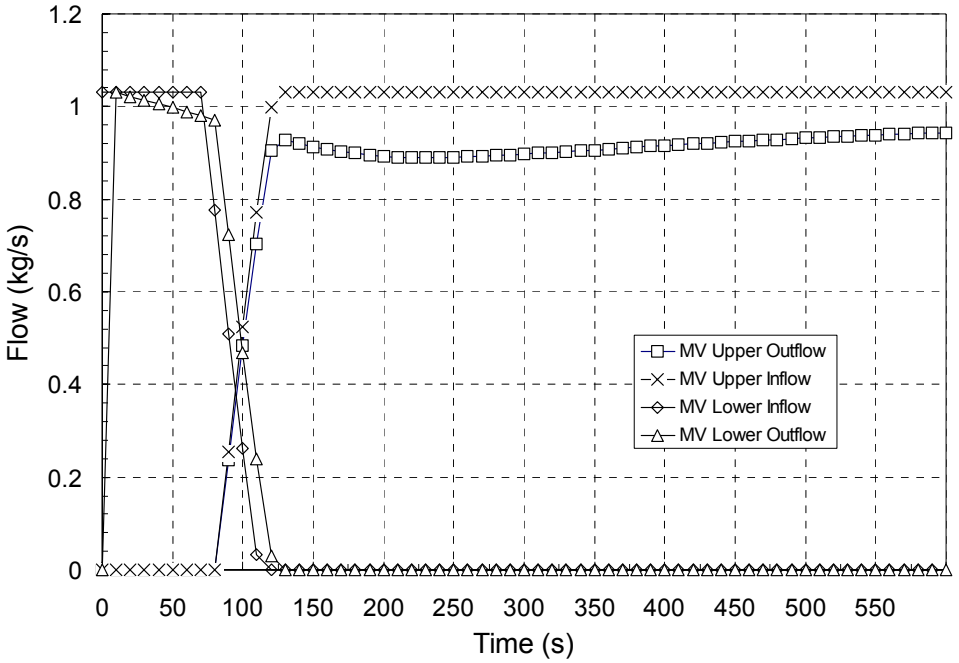

Figure 12 Mechanical Ventilation Flows – Case 5, Part I

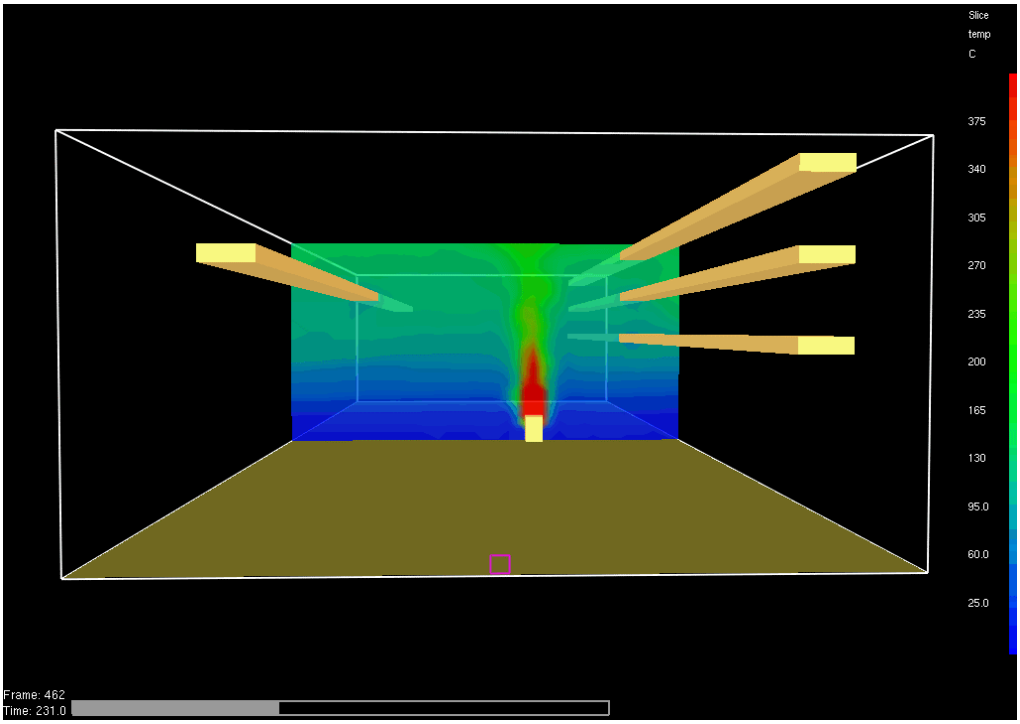

Figure 13 Temperature Profile – Base Case, Part I at 230 s

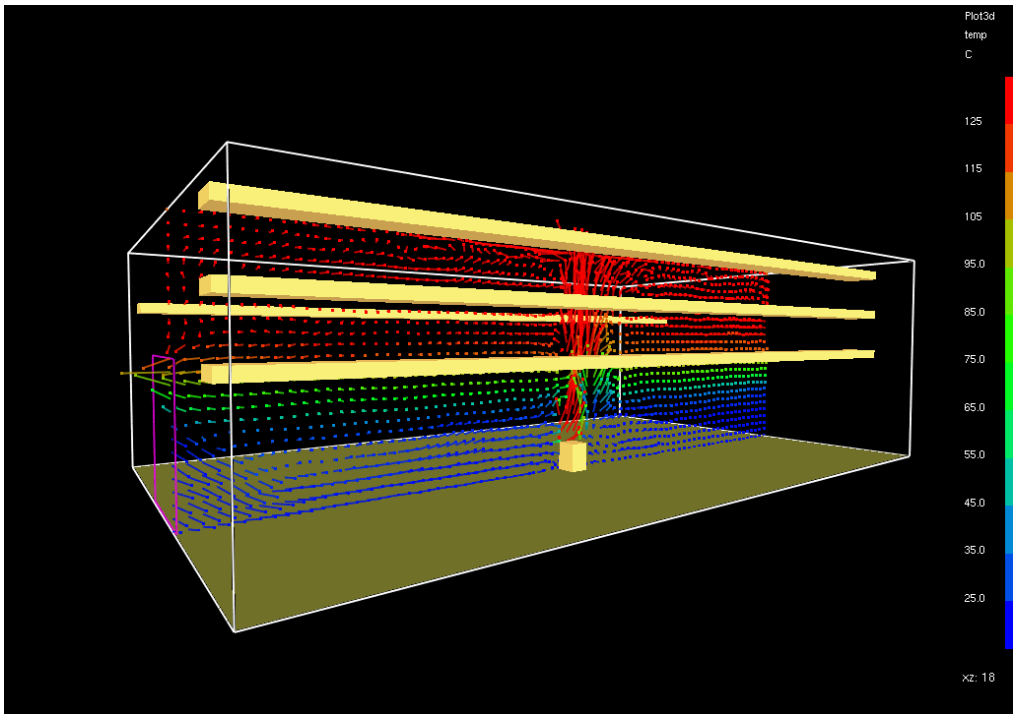

Figure 14 Door Flows – Case 4, Part I

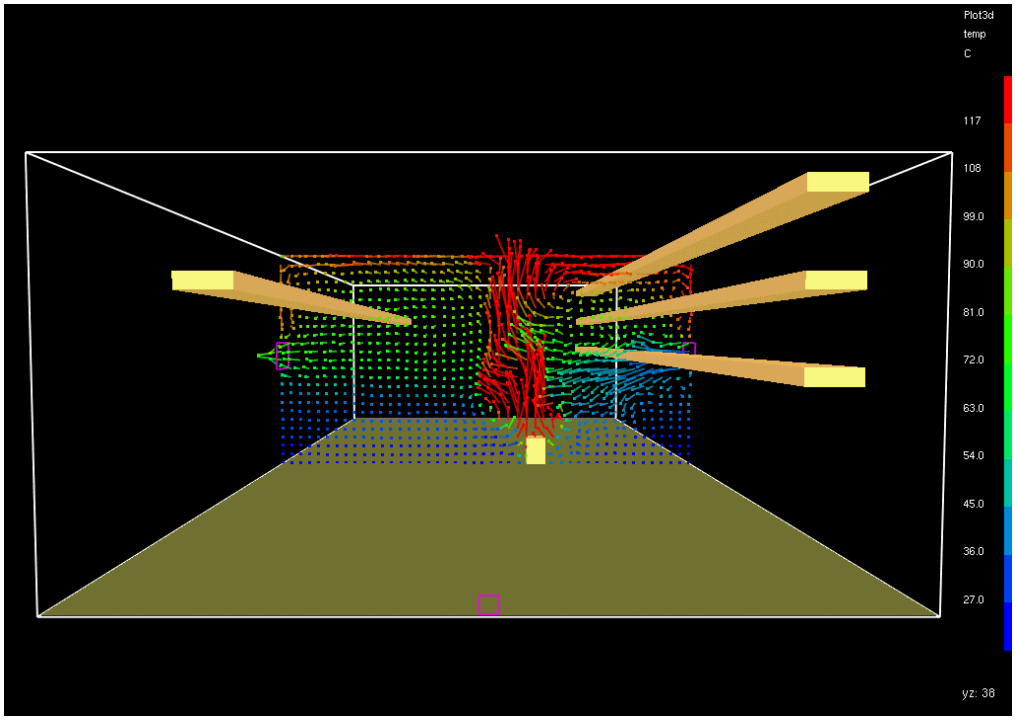

Figure 15 Effects of Mechanical Ventilation –Case 5, Part I

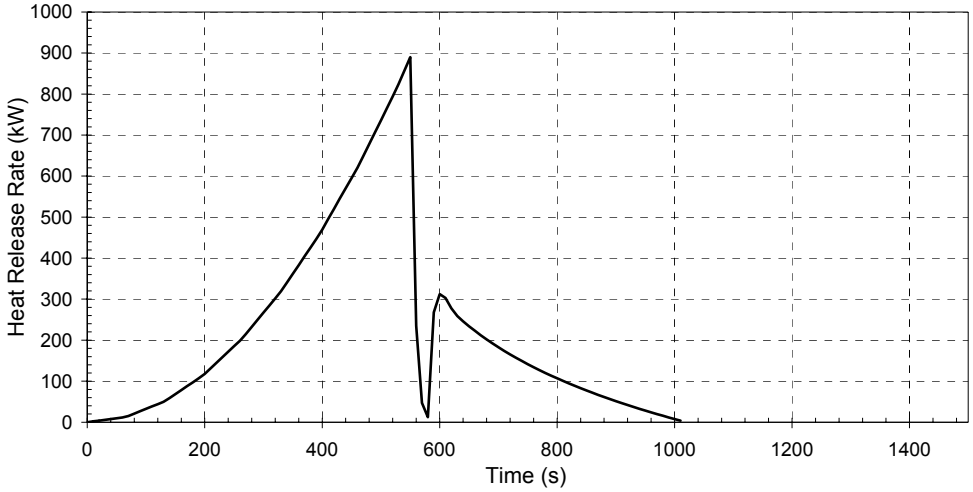

Figure 16 Heat Release Rate, Base Case, Part II

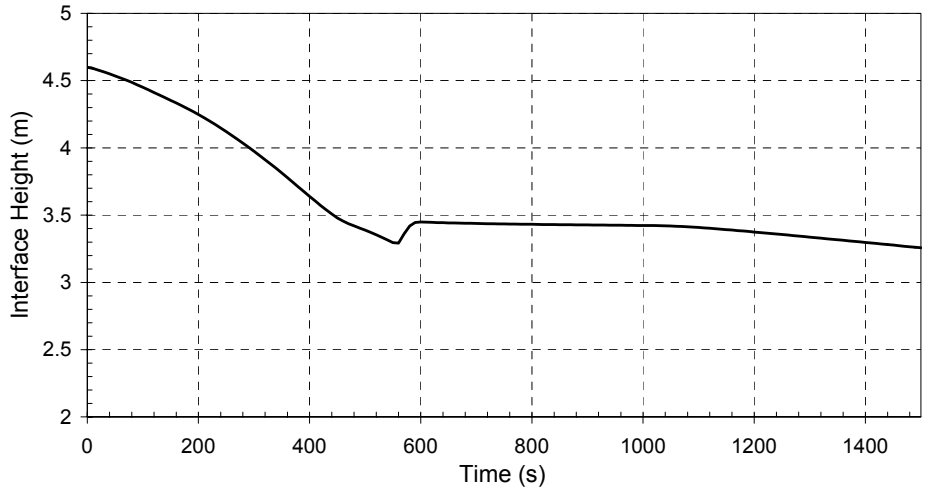

Figure 17 Interface Height, Base Case, Part II

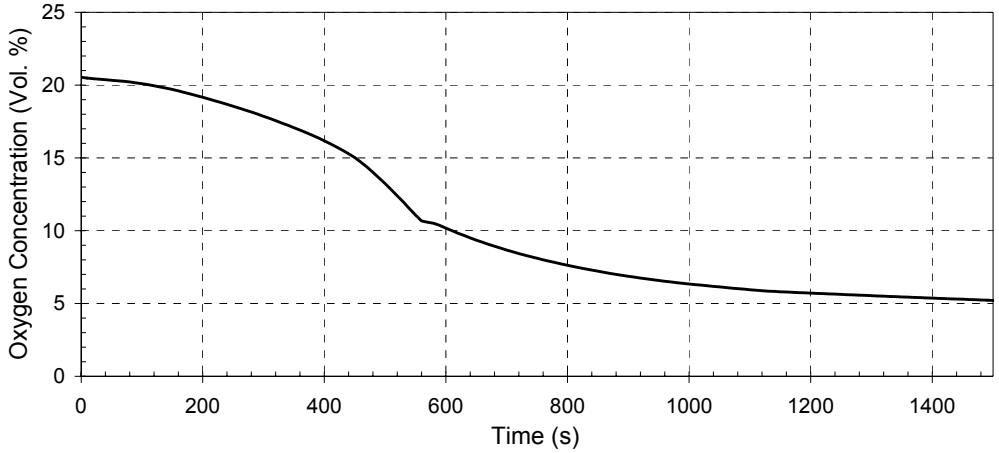

Figure 18 Oxygen Concentration, Base Case, Part II

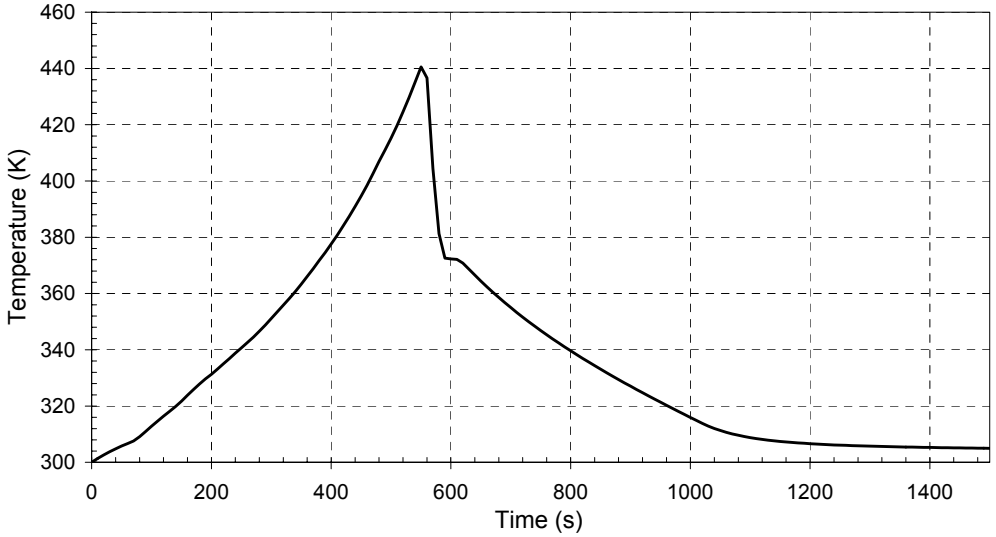

Figure 19 HGL Temperature, Base Case, Part II

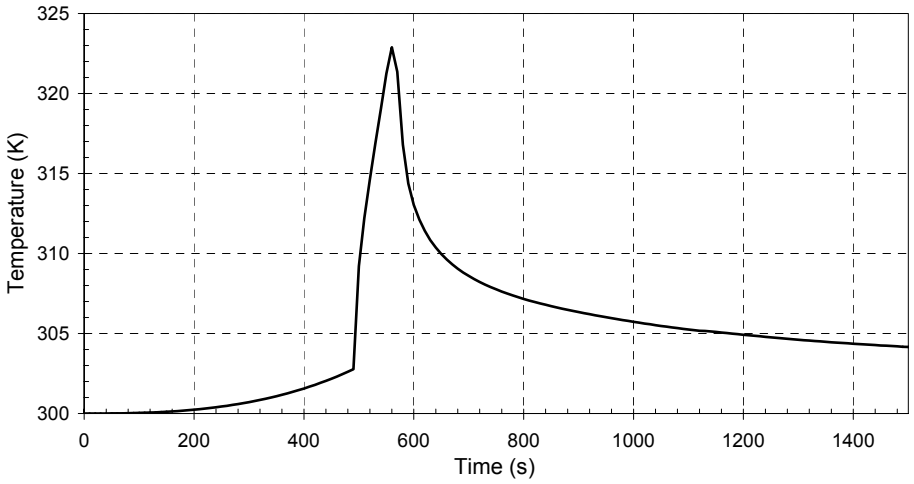

Figure 20 Target Surface Temperature, Base Case, Part II

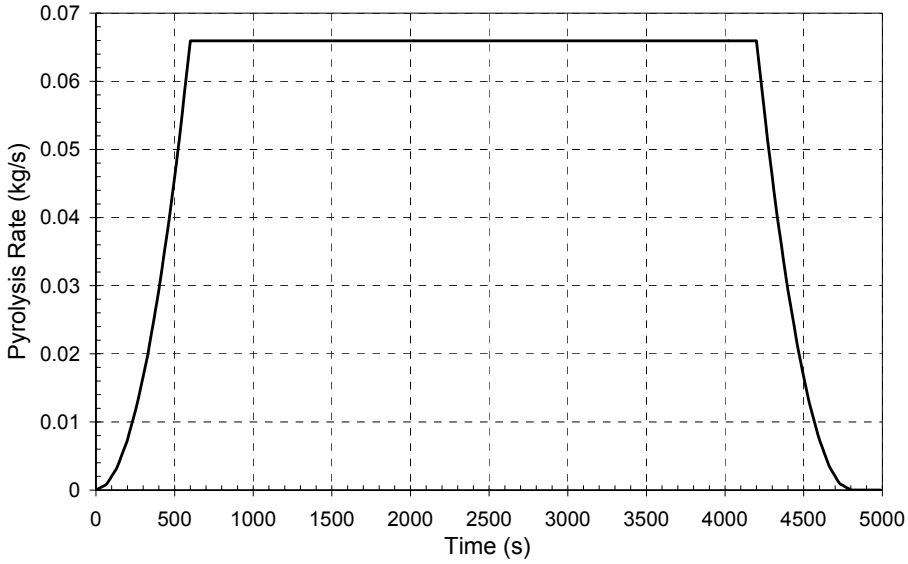

Figure 21 Pyrolysis Rate, Base Case, Part II

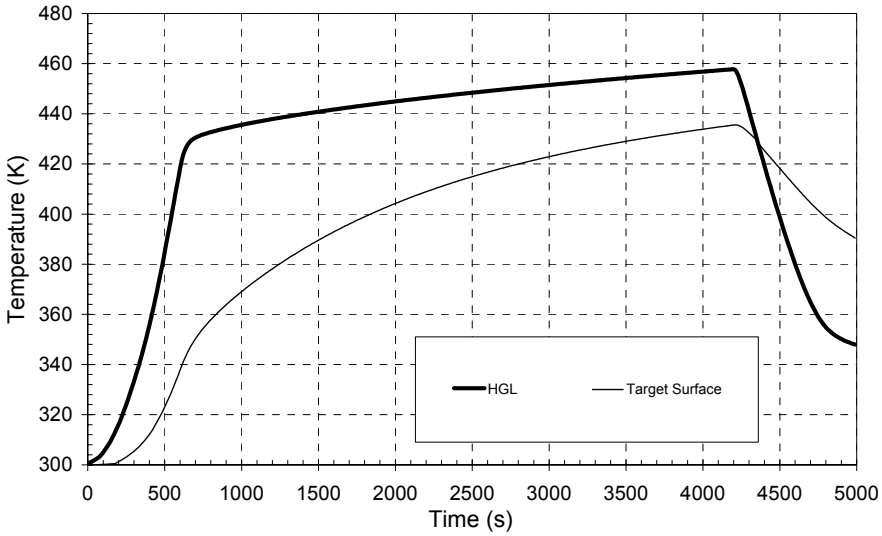

Figure 22 Temperature Development, Special Case, Part II